J. Fluid Mech. (1988), *vol.* 197, *pp.* 389–414
Printed in Great Britain

Substructures in a turbulent spot

By R. SANKARAN†, M. SOKOLOV‡ AND R. A. ANTONIA†

† Department of Mechanical Engineering, University of Newcastle, New South Wales, 2308, Australia

‡ Department of Fluid Mechanics & Heat Transfer, Tel Aviv University, Tel Aviv, 69978, Israel

(Received 27 October 1987)

Substructures within a turbulent spot which develops in a slightly heated laminar boundary layer have been identified using arrays of cold wires aligned in either a streamwise direction or in a direction normal to the wall. At any given streamwise distance from the spot origin, histograms of the number of detected substructures exhibit a peak, defining the most probable spot or the spot with the most likely number of substructures. The number of substructures in the most probable spot increases with streamwise distance but all substructures are convected at approximately the same velocity for any given distance from the wall. This velocity is approximately equal to that of the leading edge of the spot and increases slightly with distance from the wall. The increase in the number of substructures accounts for the streamwise growth of the spot. A simple relation is derived for determining the number of substructures at a particular streamwise station and a geometrical construction is proposed for identifying the origin of a new substructure. There is sufficient evidence for suggesting that the new substructures are formed near the trailing edge of the spot. The convection velocity, inclination and lengthscales of the substructures compare favourably with the corresponding characteristics of hairpin vortices.

1. Introduction

Considerable information has been obtained on the conditional- or ensemble-averaged structure of a turbulent spot: one can cite many references (e.g. Wygnanski, Sokolov & Friedman 1976; Cantwell, Coles & Dimotakis 1978; Antonia *et al.* 1981; and the relatively recent review of the current state of knowledge on spots by Riley & Gad-el-Hak 1985). The averaging, usually conditioned on either the spot trigger or a characteristic feature of the spot such as its leading edge or trailing edge†, tends to mask the internal structure of the spot. More recent experiments, using either flow visualization (e.g. Perry, Lim & Teh 1981; Gad-el-Hak, Blackwelder & Riley 1980, 1981; Matsui 1980) or arrays of either hot wires or cold wires (Wygnanski, Haritonidis & Kaplan 1979; Antonia *et al.* 1981; Wygnanski, Zilberman & Haritonidis 1982; Wygnanski 1983) have signalled the presence of many eddies or substructures within individual realizations of a spot. On the basis of flow visualizations, it has been suggested that the structures consist of hairpin eddies, sometimes Λ-vortices or vortex loops. In this respect, there appears to be significant similarity between photographs of the (x, y)-plane of a turbulent spot (Gad-el-Hak

† The terms leading edge and trailing edge are commonly used in the spot literature and are retained here. Clearly, LE and TE refer to the downstream and upstream boundaries respectively, of the spot.

et al. 1980, 1981) and the (x, y)-plane photographs of Head & Bandyopadhyay (1981) for a turbulent boundary layer. The latter authors noted that large-scale bulges in a turbulent boundary layer are made up of clusters of vortex loops, their number (or density), geometry, kinematics and, presumably, dynamics depending, to a significant degree, on the Reynolds number. Several authors, e.g. Bandyopadhyay (1983), Fleischmann & Wallace (1984) and Johansson, Her & Haritonidis (1987) have commented on the similarity between characteristics of vortex loops in a spot and those in a fully developed boundary layer.

It should also be mentioned that spanwise or (x, z)-plane views of the spot (e.g. Cantwell *et al.* 1978; Gad-el-Hak *et al.* 1980, 1981) have clearly revealed the existence of low-speed streaks aligned in the x (streamwise)-direction. The longitudinal extent and spanwise spacing, in terms of wall units, of these streaks are similar to those pertaining to the well-studied features of low-speed streaks underneath a turbulent boundary layer.

There is plausible evidence that the hairpin vortex or the double-roller eddy (Townsend 1956) is an important if not basic ingredient not only in wall-bounded flows but also free-shear flows, such as plane jets and plane wakes. Rogers & Moin (1987) conclude, on the basis of direct numerical simulations of the Navier–Stokes equations, that hairpin vortices are an important vortical structure in homogeneous as well as inhomogeneous turbulent shear flows. It is therefore important that the geometrical, kinematical and dynamical properties of these vortices are studied, with the eventual goal of elucidating their function and, more specifically, their role in transferring momentum and scalar quantities. The turbulent spot provides a relatively controlled environment for focusing and studying this vortical structure in view of the constraining influence of the spot boundaries.

The information that has so far been obtained via flow visualization on the spot substructures is limited, presumably because of the disadvantages of interpreting flow visualizations unambiguously (e.g. Gad-el-Hak, Blackwelder & Riley 1985). There have been a few attempts (Wygnanski 1983; Itsweire & Van Atta 1984) at obtaining quantitative information on the substructures. Although useful, these attempts have yielded only limited information, partly because of the nature of the data collected (e.g. Wygnanski used an array of single hot wires and Itsweire & Van Atta used a V-probe) and partly due to the use of one-point data for detecting the substructures. Nevertheless, Wygnanski's idea of constructing a statistically most probable spot (MPS), defined as the spot population with the most probable number of substructures, has merit and is retained here. This idea was used by Itsweire & Van Atta who noted that the selection of only those spots that contain a certain number of substructures is one operational means of producing identical spots. It is clear that the selection of a population of spots with identical or roughly identical features should considerably reduce the amount of jitter compared with what would exist if the complete population were considered and therefore enhance our ability to study the physics of the spot in some detail. Moreover, the results pertaining to the MPS are unlikely to be biased since the spots that are considered for analysis are those that occur most frequently.

The main aim of the present work is to identify the MPS and study its evolution in the plane of main shear. The identification procedure focuses on relatively sudden and spatially coherent changes in temperature, which appear ubiquitously on signals from an array of cold wires, aligned in either the x- or y (normal to the wall)-direction (e.g. Antonia *et al.* 1981). The MPS consists of the number of spots that contain the most probable number of coherent temperature changes, with the underlying

assumption that these changes represent characteristic features of the substructures. The construction of the MPS facilitates the study of the kinematics of the substructures, for which little information is available in the literature. Specifically, this paper considers the variation, with respect to both x- and y-directions, in the number of substructures and in their convection velocity. A comparison is made between the measured properties of the substructures and the observations, reported in the literature, on hairpin vortices. A longer-term aspect of the work is to delineate the topology of the velocity field associated with the substructures and to consider their dynamics. The present work focuses only on the kinematics of the substructures as inferred from the temperature field.

2. Experimental details

The boundary-layer tunnel used for the present investigation is of the open-return blower type. A description of the tunnel is given in Antonia, Chambers & Sankaran (1985) and, in less detail, in Sankaran, Chambers & Antonia (1986). We only give here experimental details relevant to the present investigation.

The laminar boundary layer develops on one of the vertical walls of the working section (height = 0.89 m, width = 0.15 m at the contraction exit, length = 5.4 m). The other vertical wall is adjusted to achieve a zero pressure gradient ($(2/\rho U_1^2)\,\mathrm{d}p/\mathrm{d}x \approx -2.5\times10^{-5}$ cm^{-1}, where U_1 is the nominal free-stream velocity). The boundary-layer wall is made up of three 1.27 cm thick aluminium plates, each heated by three rows of six 0.1 cm thick Sierracin pads (26×26 cm) bonded to the back of the plate. The pads are connected in series and a.c. heated using a zero-crossing variable duty cycle heater controller operated at 240 V and 10 A to achieve uniform wall heat-flux conditions. Heat losses from the back of the metal plates have been minimized by using 45 mm thick thermal insulation.

The wall temperature is continuously monitored at a number of streamwise and spanwise stations with integrated-circuit temperature transducers. These transducers are inserted in 5 mm dia. and 5 mm deep holes drilled in the back of the plate and secured in position with a highly conductive silicone compound. The output from each transducer is proportional to the absolute temperature when a constant current is maintained through the transistor junction of the transducer. These transducers were calibrated in constant-temperature baths (in the range 273 to 323 K) against a platinum resistance thermometer (least count 0.01 K).

The turbulent spot is initiated by a small jet of air issuing periodically from a 3 mm dia. hole located on the wall centreline, at a distance of 30 cm ($x_s = 0$) from the contraction exit plane. The jet is triggered by an audio speaker, mounted on the back of the aluminium wall and driven by a square wave of 15 V amplitude and a frequency of 3 Hz. The square-wave duration of 62.5 μs produces a well-developed spot at the first measuring location downstream.

Two arrays of cold wires, one with the wires aligned in the x-direction and the other with alignment in the y-direction, are used. The x-array is used for substructure convection velocity measurements and the y-array for substructure inclination measurements. Use is made of both arrays (not simultaneously) for substructure identifications. The y-array includes twelve cold wires, number and separation of wires being such as to provide adequate coverage of the full height of the spot at $x_s = 113$ cm. Three wires only are used in the x-array, with nominal separations of 14 mm and 17 mm, to maximize the accuracy of the convection velocity measurement by the transit time method (see later section). The arrays are

constructed in-house using L-shaped epoxy fibreglass circuit boards which are glued back to back. Guitar wires (dia. = 0.6 mm) of length about 20 mm are then soldered on the ends of the boards to form the wire prongs (effective length = 15 mm and separation $\approx$ 5 mm).

The cold wires are made of 0.63 μm dia. Wollaston wires (Pt–10% Rh) soft soldered on the prong tips. A length of about 1 mm is etched from the central part of the wire. Each wire is operated by a constant-current circuit (0.1 mA) as a resistance thermometer. The temperature coefficient of the wires (0.0016 K^{-1} $\pm$5%) is estimated by calibration at the exit plane of a heated air jet. Voltages from the constant-current circuits are digitized at a maximum sampling frequency of about 36 kHz for the x-array and 16 kHz for the y-array (for all channels) using a 16 channel data acquisition system (12 bit A/D converted) connected to a PDP 11/34 computer. A higher sampling frequency was used with the x-array to obtain accurate estimates of the convection velocity of the substructures (§6). The square wave was always digitized and used for the purpose of reference. The data are stored on mag tape and processed on a VAX 11/780 or VAX 11/8550 computer. Record durations of 120 s contained approximately 400 spots for the x-array and 450 spots for the y-array.

The arrays were mounted on a traversing unit (Mitutoyo height gauge, least count of 0.01 mm). The distance from the wall was determined optically by viewing the wire and its reflection in the polished aluminium surface through a theodolite. The uncertainty in determining the distance using this procedure is estimated to be $\pm$0.02 mm.

Measurements have been made on the centreline of the spot at three distances from the disturbance (nominally, x_s = 52.5, 83 and 113 cm) for U_1 = 4.3 ms^{-1}. At these stations, the difference $T_w - T_1$ (T_w and T_1 are the wall and free-stream temperatures respectively) is equal to 9.4, 9.8 and 10 K respectively. To check the quality of the laminar boundary layer, velocity and temperature profiles were measured at several values of x_s, without the spot. The resulting distributions (see Sankaran *et al.* 1986) for zero pressure gradient indicated reasonable agreement with the theoretical Blasius and Pohlhausen distributions. At $x_s = 0$, the measured laminar boundary-layer thickness (δ_ℓ) and the thermal-layer thickness are 5.5 mm and 5.3 mm respectively. The corresponding displacement and momentum thicknesses are 1.9 mm and 0.76 mm respectively, while the enthalpy thickness is 0.72 mm.

For a nominal value of $(T_w - T_1) = 9.4$ K at $x_s = 52.5$ cm, the ratio Gr/Re^2 or Richardson number (Gr is the Grashof number $g\delta^3(T_w - T_1)/\nu^2 T_1$ and Re is the Reynolds number $U_1\delta/\nu$, where δ is the boundary-layer thickness and ν is the kinematic viscosity) is about 10^{-4}. When the Grashof and Reynolds numbers are based on velocity, length and temperature scales defined at the edge of the sublayer instead of the edge of the boundary layer, the ratio Gr/Re^2 is appropximately 5×10^{-5}. The previous estimates indicate that buoyancy effects are negligible everywhere in the flow.

No effort has been made to reduce the turbulent contamination (e.g. Motohashi & Blackwelder 1983) arising from the sidewalls. However, cursory measurements made (without the spot) by traversing a single hot wire in the z (spanwise)-direction at different x-stations, indicated that the contamination grows away, at about 9.2° with respect to x, from the upper and lower horizontal walls of the working section. Using this angle, the sidewall contamination would reach the centreline of the tunnel at $x_s \approx 170$ cm. The last measurement station used in these experiments is at x_s = 113 cm.

3. Detection of substructures

The strategy adopted for the construction of the MPS consists in using temperature as a passive marker of characteristic features of the substructures. Antonia *et al.* (1981) observed that simultaneous temperature traces, obtained with a y-array of four cold wires, indicated the existence of several coherent structures within one spot. Although the number of wires was small, the traces clearly revealed a signature similar to that observed in a turbulent boundary layer (e.g. Chen & Blackwelder 1978; Subramanian *et al.* 1982). This signature is also evident in the traces of figure 1 (*a*) (x-array) and figure 1 (*b*) (y-array); it is characterized by a relatively slow increase in temperature followed by a more sudden decrease. Both heatings and coolings can be traced across the full height of the spot (figure 1*b*). In particular, figure 1 (*b*) indicates that this signature is recognizable at the location of the wire closest to the wall, implying that the structure that causes this signature originates near the wall. The cooling was associated with the back of a bulge in the outer part of the boundary layer (by Chen & Blackwelder 1978) and Antonia *et al.* (1981) speculated that the signature could be associated with hairpin vortices. It seems plausible, for the present purpose, to associate the cooling with the upstream or trailing edge of a substructure and to tentatively identify the heating with the downstream or leading edge of the substructure. The algorithm used for detecting substructures can focus on either coolings or heatings, although the results presented in later sections will pertain mainly to coolings.

Before searching for substructures, the leading edge and trailing edge of the spot are identified. These locations essentially correspond to the downstream and upstream laminar/turbulent interfaces of the spot. These interfaces are more likely to be interpreted as envelopes of the heads of the substructures than as themselves belonging to the substructures. Accordingly, they have been ignored in the present substructure detection scheme.

To determine the leading edge and trailing edge of the spot, the following criteria were applied:

$$\left|\theta_j - \frac{1}{d}\sum_{i=j-1}^{j-d}\theta_i\right| > k\theta'_{\mathrm{t}} \quad \text{(for leading edge)}, \tag{1}$$

and

$$\left|\theta_j - \frac{1}{d}\sum_{i=j+1}^{j+d}\theta_i\right| > k\theta'_{\mathrm{t}} \quad \text{(for trailing edge)}. \tag{2}$$

Here θ_j is the jth sample of the digital time series for the instantaneous temperature, d is the width of the averaging interval, k is a threshold parameter and θ'_{t} is an approximation to the r.m.s. value for only the turbulent part of the temperature signal. To estimate θ'_{t}, the following method was used. The probability density function of the total (laminar + turbulent) signal showed a distinct narrow peak corresponding to the laminar portion of the signal. The r.m.s. of only those data whose values were outside this peak was taken as θ'_{t}. (In all cases, this estimate was close to the true turbulent r.m.s. value, subsequently obtained from the data falling within the spot boundaries identified by this procedure.) The first sample at which (1) is first satisfied defined the leading edge. The trailing edge is identified with the last sample at which (2) is satisfied; here, 'last' means that (2) is required to fail at each of the following 200 samples. Examples of leading edge and trailing edges identified in this manner are shown in figure 1 (*a*, *b*) for one spot.

Values of k and d were initially selected such that good agreement between the

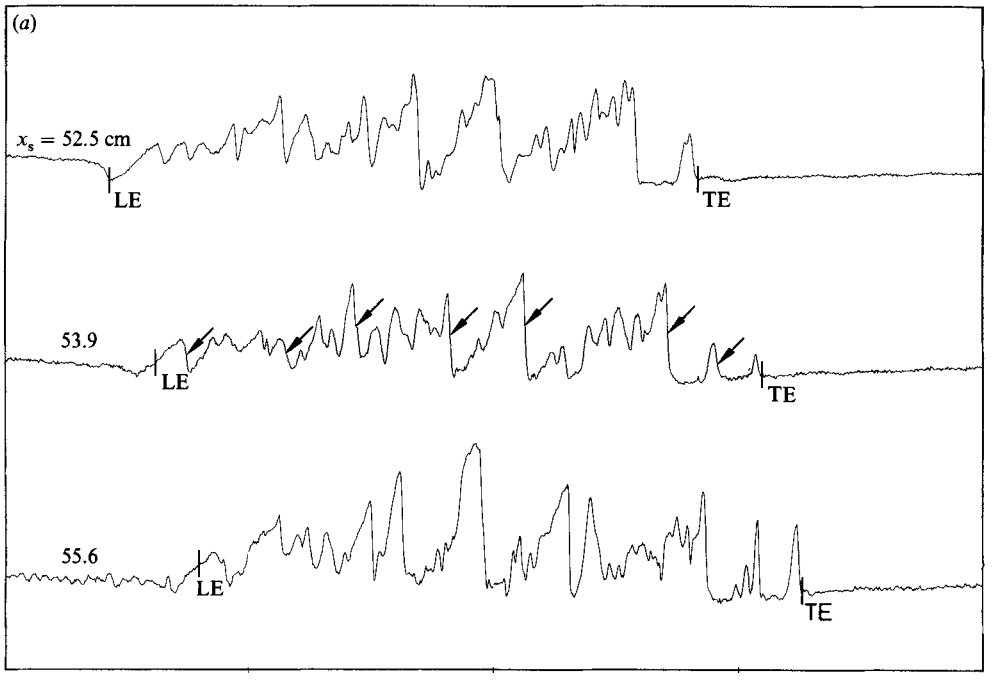

FIGURE 1 (*a*). For caption see facing page.

detection positions and the computer plot of temperature traces was obtained. To check the dependence of the detection positions on k and d, a particular value of d was first chosen (= 10 samples, or 1.12 ms) and k was varied until the leading- and trailing-edge positions (as well as the time difference between these locations) became constant. In the present experiment, such a plateau was found for $0.45 < k < 0.75$. For a value of $k = 0.5$, it was subsequently found that, for $8 < d < 14$, the leading- and trailing-edge locations did not change. The final values of k and d were 0.5 and 10 samples respectively.

In the present multipoint detection scheme, a computation window of size $(2\tau + 1)$ data samples is moved sample by sample through the digital record of temperature obtained at one location from the array (say, wire 2 of the x-array). A window average gradient (WAG) is then calculated where

$$\mathrm{WAG}_j = \frac{\mathrm{sign}}{2\tau}\left(\sum_{i=j+1}^{j+\tau}\theta_i - \sum_{j-\tau}^{j-1}\theta_i\right) \tag{3}$$

where the centre of the window is at $i = j$ and sign has a value of either -1 or $+1$ depending on whether coolings or heatings are sought. A provisional detection is recorded for each patch of the digital record, defined as follows: (i) the patch begins when the value of WAG_j first exceeds $k_1\theta_2'$, where k_1 is a threshold parameter and θ_2' is the r.m.s. value of the turbulent part of the θ_2 temperature record of wire 2; and (ii) the patch ends when WAG_j next falls below zero. The provisional detection instant is that value of j within the patch for which WAG_j is largest. After a provisional detection ($j2$) on wire 2 is found, the records θ_1 and θ_3 of wire 1 and wire 3 are searched over a short time, t_d, before and after $j2$ to find the maximum

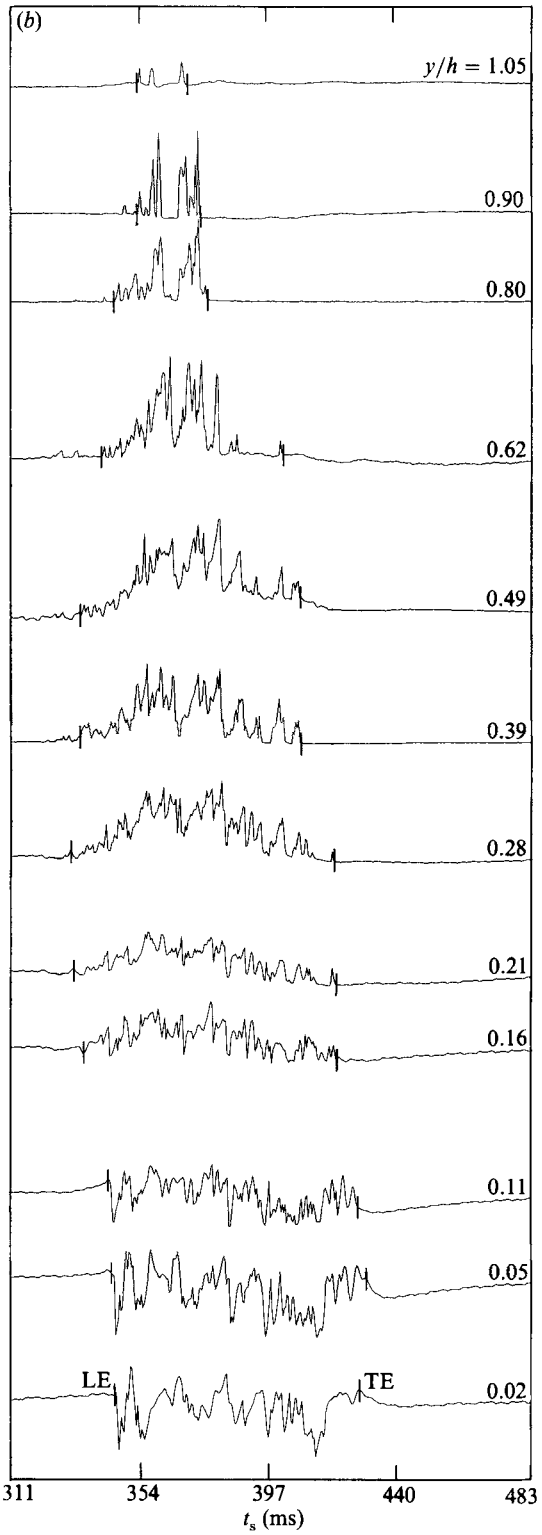

FIGURE 1. Temperature signals for one spot from the arrays of cold wires: (*a*) x-array, $y/h = 0.085$; (*b*) y-array, $x_s = 113$ cm.

WAG_j instants ($j1$ and $j3$ on wires 1 and 3 respectively) for each signal. An average signal is then formed such that $j1$, $j2$ and $j3$ are coincident, i.e. for $-\tau \leqslant t \leqslant \tau$

$$T_{\mathrm{av}}(t) = \tfrac{1}{3}[\theta_1(j1+t)+\theta_2(j2+t)+\theta_3(j3+t)]$$

WAG_j is then recalculated for this average signal and the provisional detection is accepted as final if $\mathrm{WAG}_j > k_1\theta_2'$. Note that the formation of T_{av} ensures that detections are based on features that have a significant spatial extent.

The precise magnitudes of $(2\tau+1)$ and t_{d} are not critical. Here, $(2\tau+1)$ is set to 31 samples, approximately half the number of samples corresponding to the period of the feature being detected. A value of 60 samples is chosen for t_{d} after visual examination of temperature signal traces. This was sufficient to allow for the different arrival times of the desired feature at the cold wires of the array. An objective choice of k_1 is not simple; we found however, that $k_1 = 0.3$ gives satisfactory detection, as indicated for example by the arrows in figure 1(*a*).

4. Construction of MPS

Histograms of the number of substructures present within each spot were constructed for the total number of spots at three values of x_{s} and several distances from the wall. Figure 2 shows the results for a particular value of y. The histogram at each x_{s} shows a distinct peak, here identified with the MPS, i.e. with the spot population that contains N_{p}, the most probable number of substructures. Histograms of the number of substructures were also calculated from the y-array data with a detection procedure similar to that used for the x-array data. These latter histograms yielded the same N_{p} as that obtained with the x-array for the same y, thus providing a useful consistency check of the detection procedure. Figure 2 also shows a significant increase in N_{p} as x_{s} increases, from 7 at $x_{\mathrm{s}} = 52.5$ cm to 13 at $x_{\mathrm{s}} = 113$ cm. The duration of the spot, as defined by $(t_{\mathrm{TE}} - t_{\mathrm{LE}})$, where t_{TE} and t_{LE} are the most probable arrival times of trailing and leading edges respectively, increases by about 100% between $x_{\mathrm{s}} = 52.5$ and 113 cm. It seems reasonable to associate this increase with the increase in N_{p}. The histograms in figure 2 also indicate that there is a significant population of spots that contain $N_{\mathrm{p}}+1$ and $N_{\mathrm{p}}-1$ substructures. These populations are designated by MPS+1 and MPS−1 in figure 2 for $x_{\mathrm{s}} = 52.5$ cm.

For a particular value of x_{s}, the histograms in figure 3 show that N_{p} tends to decrease as y/h† increases, except perhaps in the vicinity of the wall. This is best illustrated by plotting $N_{\mathrm{p}}/N_{\mathrm{p}}^*$ in terms of y/h (e.g. figure 4). N_{p}^* is the largest value of N_{p} for any given x_{s}. Two general features emerge from figure 4. First, there is a significant near-wall region, for which $N_{\mathrm{p}}/N_{\mathrm{p}}^*$ is unity. For $y/h \gtrsim 0.2$, there is a significant decrease in $N_{\mathrm{p}}/N_{\mathrm{p}}^*$ towards the edge of the spot. This decrease does not imply that the actual number of substructures depends on y/h; it simply reflects the likelihood that individual substructures have different heights (the height of a substructure is defined as the maximum distance it extends away from the wall). The traces of figure 1(*b*) suggest that the height of the substructures near the centre of the spot will be larger than those near trailing or leading edges. Secondly, the data in figure 4, although constrained to a maximum of unity owing to the normalization by N_{p}^*, tend to follow the same distribution, independently of the value of x_{s} at which they are obtained. The height h of the spot has been found to be an appropriate

† h is the height of the spot, here defined as the maximum value of y for the contour $\tilde{T}/(T_{\mathrm{w}}-T_1) = +0.03$, where $\tilde{T}$ is the ensemble-averaged temperature defined as in Antonia *et al.* (1981).

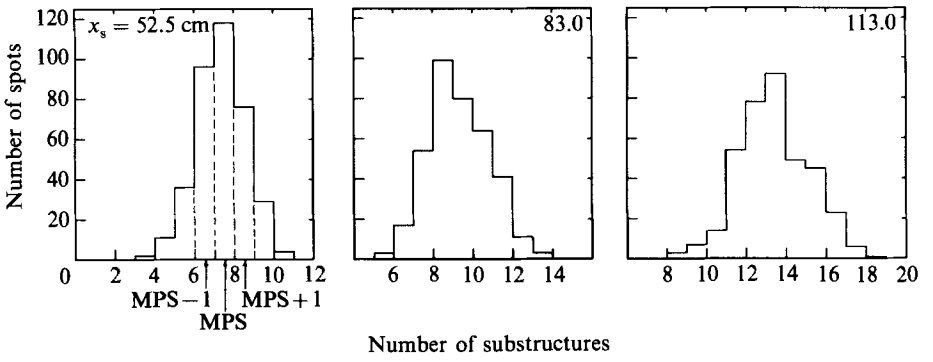

FIGURE 2. Histograms for the number of substructures within a spot at $y = 2.9$ mm but for different x_s.

similarity parameter for describing the global growth of the spot (e.g. Sokolov, Antonia & Chambers 1980). Ensemble-averaged properties of the spot, obtained for experimental conditions similar to those used here, were adequately described in terms of the normalized variables $x_s/U_1 t_s, y/h, z/z_{max}$ (Sankaran & Antonia 1988). Figure 4 corroborates the appropriateness of h as a similarity scale.

Note that the data of figure 4 (*a*), obtained from the x-array, are in close agreement with those in figure 4 (*b*), where the y-array is used. Note that the data of Wygnanski (1983) who used a y-array of hot wires and detected 4–5 substructures ($x_s = 37.5$ cm, $U_1 = 6$ m/s) are in good agreement with the present data. In Wygnanski's scheme, the detections were identified with local minima in low-pass-filtered velocity signals, after the latter fell below an arbitrary threshold. The distribution of the substructures at several values of y/δ_ℓ was presented in the form of histograms. For the purpose of comparison, the number of substructures corresponding to the peak of each histogram is taken as N_p, and the height of the spot was inferred from the approximation of Wygnanski *et al.* (1982) that the spot growth in the y-direction is about 0.8 of the turbulent boundary-layer thickness developing from the location of the disturbance and has the same initial thickness as the laminar boundary layer at that location.

Since the local temperature changes should be associated with velocity changes (e.g. a cooling, $d\theta/dt < 0$, should correspond to a local acceleration $du/dt > 0$), the velocity-based detection used by Wygnanski is expected to yield results similar to those obtained with the present temperature-based approach. Nonetheless, the degree of agreement indicated in figure 4 (*b*) between the two results gives encouraging support to the notion of a universal structure for the MPS.

Histograms of detection times† of individual substructures are shown in figure 5 for $x_s = 52.5$ cm and $y/h = 0.71$. In this figure, the times are calculated with respect to the LE, in order to eliminate any jitter associated with the arrival time of individual realizations. These histograms highlight the existence of each substructure since three relatively distinct peaks, of nearly equal magnitude, can be recognized, corresponding to the three substructures indentified in histograms similar to those shown in figure 3. When the entire spot population is considered (figure 5*b*), the histograms of detection times show only one peak, which corresponds to a relatively small time (the first substructure is presumably always recognized). The difference

† These times correspond to coolings, but similar histograms have been obtained when the detection focuses on heatings.

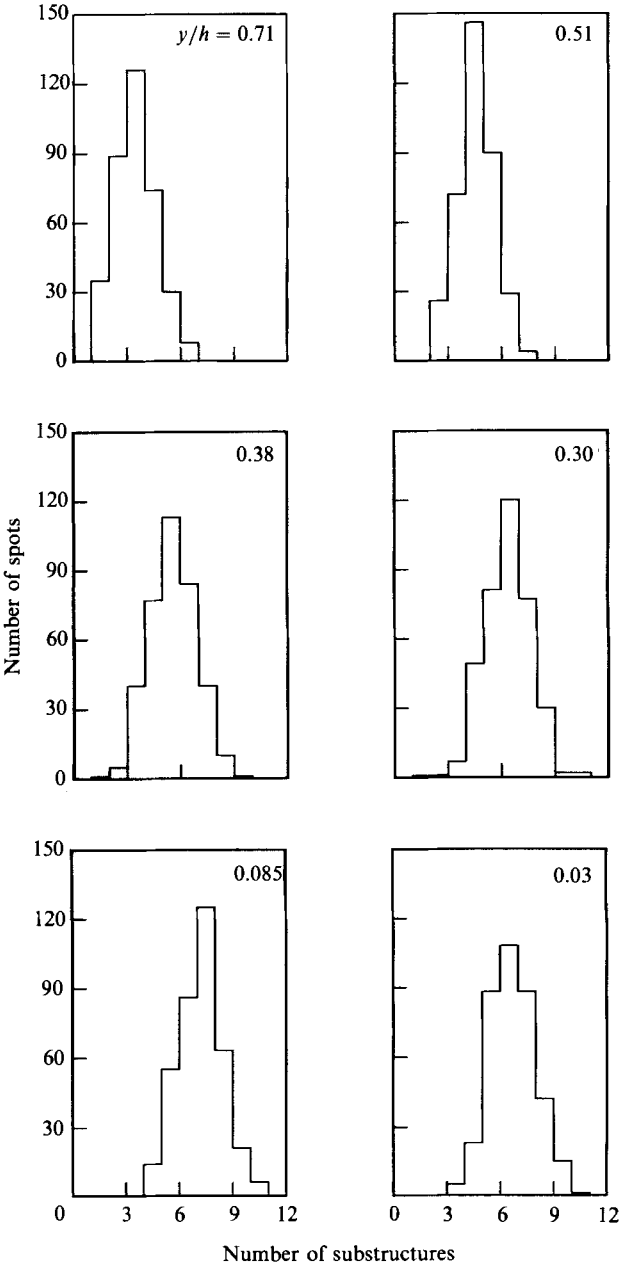

FIGURE 3. Histograms for the number of substructures at $x_s = 52.5$ cm but for different y/h.

between figures 5(*b*) and 5(*a*) reflects, to a large extent, the jitter in the arrival times of the physical structures that make up the spot. This jitter is much less severe when we restrict our attention to the MPS (figure 5*a*); it is nevertheless evident that the MPS population is not entirely jitter-free. The selection of only these spots that contain the most likely number of features lends itself well to the further detailed analysis of these features. The results in the following sections relate only to the MPS.

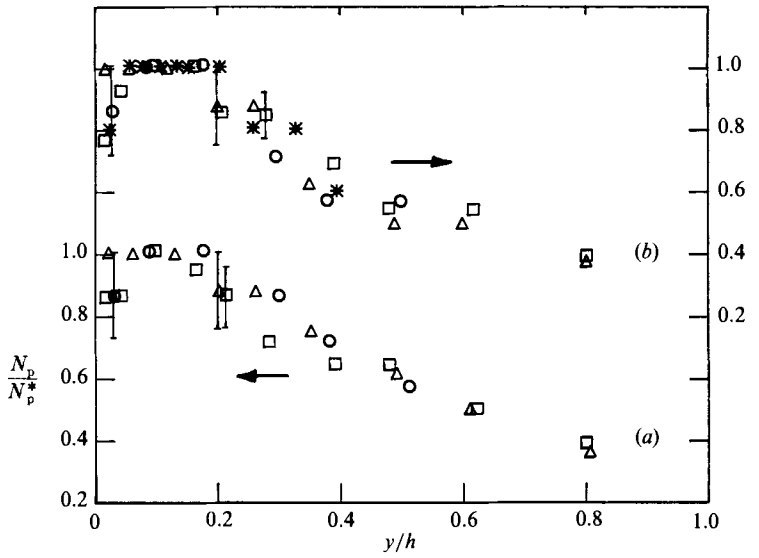

FIGURE 4. Dependence of the number of substructures in the MPS on distance from the wall: (*a*) *x*-array; (*b*) *y*-array. ○, $x_s = 52.5$ cm; △, 83; □, 113; *, calculated from the data of Wygnanski (1983).

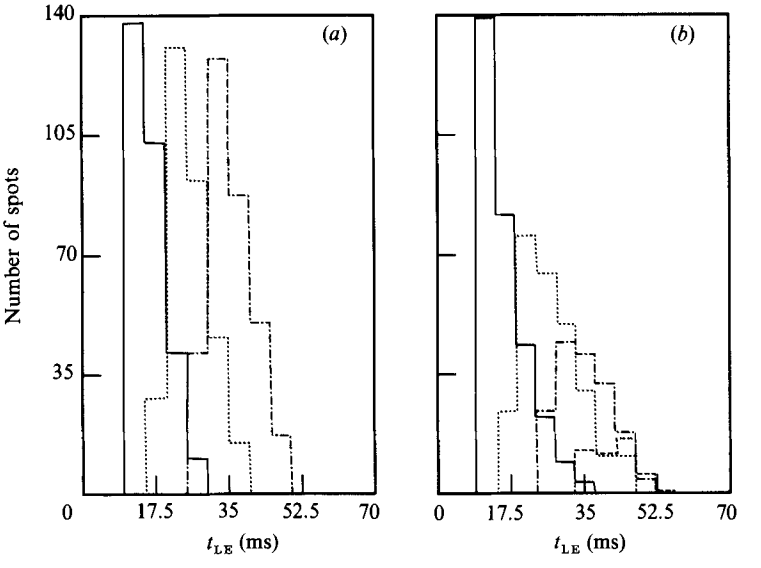

FIGURE 5. Histograms of the detection times of the MPS substructures relative to the spot leading edge: (*a*) MPS; ——, substructure 1; · · ·, 2; —·—, 3. (*b*) Entire population; ——, substructure 1; · · ·, 2; —·—, 3; — —, 4.

5. Characteristics of substructures

In this section, we consider several characteristics of the substructures: convection velocity and origin, streamwise spacing and inclination.

5.1. *Convection velocity*

The histograms of the detection instants for the MPS (figure 5*a*) cannot, on their own, be used for inferring the velocity of the individual substructures. One cannot, for example, assume that the substructures originate at $x_s = 0$, the effective origin of the spot. Such an assumption would imply that different substructures travel at different velocities; relative to a fixed observer, the first substructure would travel with a velocity close to that of the spot leading edge and the last substructure with a velocity near that of the spot trailing edge. Such a variation is not corroborated by direct estimates of the convection velocity presented below.

The convection velocity of a substructure can be determined by a transit-time method, i.e. by estimating the time taken by the substructure to travel a given distance. Specifically, the most probable time taken by a substructure to travel the distance between any two of the three wires of the x-array is determined. This time corresponds to the mean of the values within the peak in histograms such as shown in figure 6 and is essentially equal to the average time. The histograms of the time delay between wire 1 and wire 2 of the x-array at $x_s = 52.5$ cm, $y/h = 0.085$ is shown for all seven substructures, which indicates that the location of the peak is essentially at the same time instant for each substructure, implying that the substructures are being convected at the same velocity.

The most probable convection velocity of each substructure, for the three values of x_s, is plotted in figure 7 for nominally the same value of y/h. The percentage variation in y/h in figure 7 (*a*) is approximately the same as in figure 7 (*b*). However, the corresponding convection-velocity variation would be larger near the wall (cf. figure 8) presumably accounting for the larger scatter in figure 7 (*a*). It is nevertheless clear that the velocity remains constant, independently of x_s. The uncertainty bars shown in figure 7 have been estimated, using the method of propagation of errors (20:1 odds), from uncertainties in the transit time (typically $\pm 5\%$) and in the separation ($\pm 1\%$).

Figure 7 also indicates that U_c/U_1 is larger at the larger value of y/h. The variation of the convection velocity with y/h is illustrated in more detail, for three values of x_s, in figure 8. Here, each data point represents the convection velocity averaged over all the substructures of the MPS, i.e.

$$\bar{U}_c = \sum_{i=1}^{N_p} U_{ci}/N_p.$$

The collapse of the data at the three stations is quite good. Figure 8 is therefore consistent with similarity when h is identified with the similarity lengthscale.

The most probable arrival times of substructures at the x_s locations are shown in figure 9 for $y/h = 0.085$. This particular y/h location falls in a region (figure 4) where N_p is constant and maximum. Numbers, instead of symbols, are used to refer to substructures at any x_s location. Within the uncertainty in t_s, parallel lines can be drawn through the same numbers. Interestingly, the slope of these lines ($0.86 \pm 6\%$) is approximately equal to the magnitude of U_c, the local convection velocity (e.g. figure 8), at the corresponding y/h-value. This tends to suggest that the convection velocity of the substructures remains constant over a significant streamwise distance

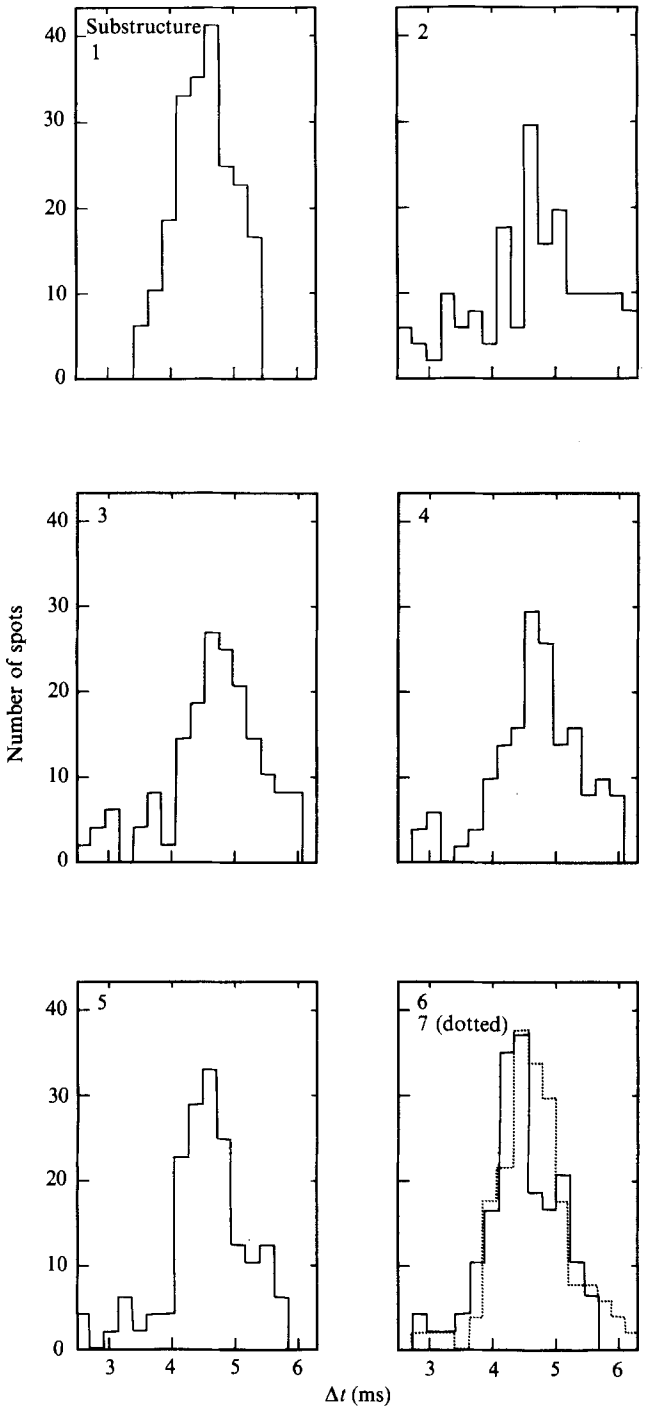

FIGURE 6. Histograms of the time delay between wire 1 and wire 2 for the seven substructures in the MPS. $x_s = 52.5$ cm.

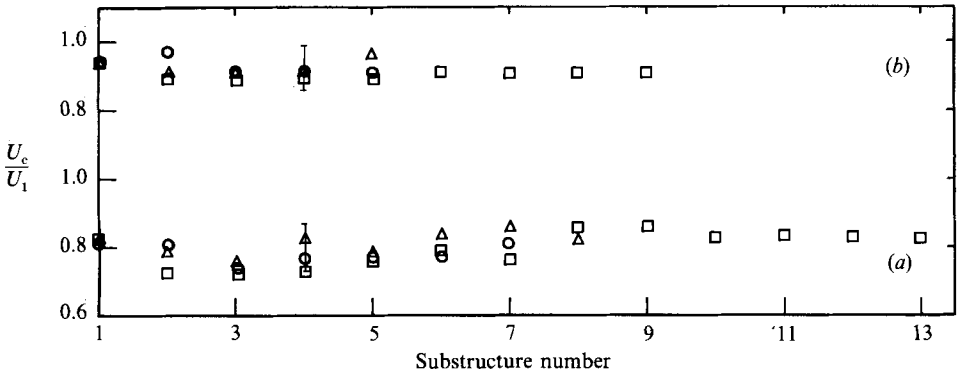

FIGURE 7. Convection velocity of different substructures of the MPS. (*a*) ○, $x_s = 52.5$ cm, $y/h = 0.085$; △, 83, 0.12; □, 113, 0.097. (*b*) ○, $x_s = 52.5$ cm, $y/h = 0.38$; △, 83, 0.39; □, 113, 0.39.

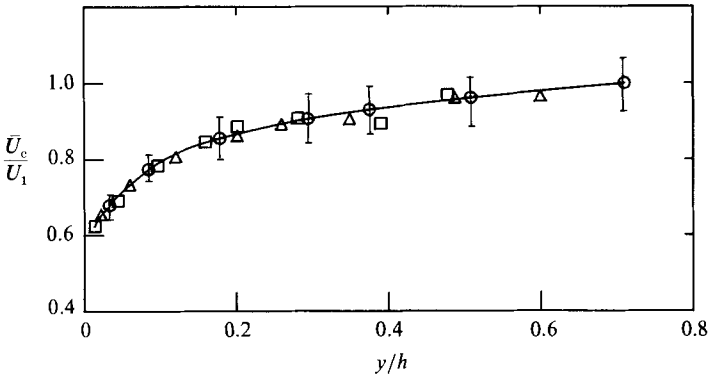

FIGURE 8. Variation of convection velocity, averaged over all substructures of the MPS, with distance from the wall. ○, $x_s = 52.5$ cm; △, 83; □, 113.

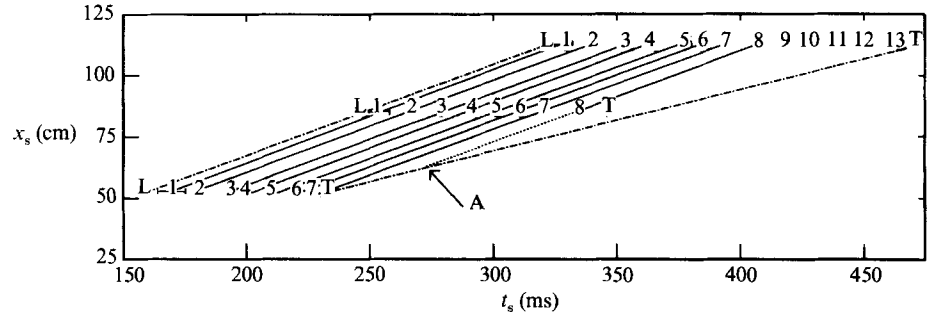

FIGURE 9. Most probable arrival times for substructures of the MPS. L, leading edge of the spot; T, trailing edge of the spot. Substructure numbers are shown at the three x_s locations.

although, evidently, one cannot guarantee that a substructure with the same number at different x_s is actually the same substructure. Note that the eighth substructure at $x_s = 83$ cm, appears to travel at the same convection velocity as substructures 1–7.

Also shown in figure 9 are the most probable arrival times of the leading edge and trailing edge of the spot. The slopes of the corresponding (broken) lines indicate that U_{LE} is $0.8U_1$ while U_{TE} is $0.58U_1$. These values are in reasonable agreement with those reported in the literature (cf. Gutmark & Blackwelder 1987, for values of U_{LE} and U_{TE} obtained by different investigators). The difference between U_{LE} and U_{TE} simply reflects the streamwise elongation of the spot as x_s increases and does not imply a decrease in the convection velocity of substructures towards the trailing edge. The elongation of the spot is due to the appearance of new substructures that travel at the same convection velocity. It is possible to estimate an average location for the origin of the new substructures using the information in figure 9. For example, in figure 9, the origin of the eighth substructure may be estimated by extrapolating the line joining the numbers 8 until it intersects the trailing-edge locus. The intersection point, labelled A in figure 9, yields the (t_s, x_s) coordinates of the origin.

5.2. *Streamwise spacing*

An approximate estimate of the interval between consecutive substructures can be inferred from figure 9. A more accurate estimate of this time can be obtained from histograms of the time duration between successive detections of coolings. A value of about 10.5 ms (± 0.7) is obtained for t_D, the most probable time, independently of which pair of successive coolings is used. Histograms constructed at different values of y and x_s show that this value of t_D is independent of x_s and y.

The streamwise spacing λ_x between substructures is equal to $t_D \bar{U}_c^*$, where $\bar{U}_c^*$ is the convection velocity of a substructure close to the wall (here, taken from figure 7 as $0.66U_1$ at $y/h = 0.02$). The present data for λ_x, normalized using different scales, are shown in table 1, together with the data of Wygnanski (1983) and Itsweire & Van Atta (1984).

The present value (≈ 280) for λ_x^+ falls well between the value of 200 reported by Falco (1977) for typical eddies in a low-Reynolds-number ($R_\theta < 1000$, where R_θ is the momentum-thickness Reynolds number) turbulent boundary layer and the value of 500, estimated by Head & Bandyopadhyay (1981) in the context of hairpin vortices, in a turbulent boundary layer ($R_\theta > 2000$).

Since t_D and $\bar{U}_c^*$ are essentially independent of x, the ratios λ_x/h and λ_x/δ_ℓ decrease (present data) with x_s. The present values of λ_x/δ_ℓ compare favourably with the range of 1.5–3.5 reported by Fleischmann & Wallace (1984) for $\bar{T}\bar{U}/\delta$, where $\bar{T}$ is the mean period of organized structures in transitional and developed bounded turbulent flows, $\bar{U}$ is the local mean velocity and δ is the local shear-layer thickness. Whereas Wygnanski's data are generally in reasonable agreement with the present results, Itsweire & Van Atta's normalized values of λ_x tend to be high, apparently because of too small a value of N_p^*.

Bandyopadhyay (1983) speculated that the mean semi-angle ϕ of the spot arrowhead is a measure of the ratio of spanwise spacing to streamwise spacing, i.e.

$$\phi = \tan^{-1}(\lambda_z^+/\lambda_x^+),$$

and indicated a value of 11.3° for his turbulent boundary-layer measurements. Using $\lambda_z^+ = 86$, the value quoted by Cantwell *et al.* (1978), and $\lambda_x^+ = 282$, we obtain a value

		Itsweire & Van Atta (1984)	Wygnanski (1983)	Present
x_s (mm)	Distance from the spot generator	600	375	525; 830; 1130
U_1 (ms^{-1})	free-stream velocity	8.6	6	4.3
$\bar{U}_c^*/U_1$	Ratio of convection velocity of a substructure† to free-stream velocity	—	—	0.66
δ_ℓ	Local laminar boundary layer thickness	6.7	8.3	8.8; 10.2; 11.8
h (mm)	Spot height	20	19	16.5; 24.0; 30.0
N_p^*	Maximum number of substructures	4–5	4–5	7; 8; 13
t_D (ms)	Most probable duration between successive boundary layers	6–7	8	10.5 ± 0.7; 10.9 ± 0.6; 11.0 ± 0.7
λ_x (mm)	Most probable streamwise spacing	40	32	30 ± 2; 31 ± 2; 31 ± 2
λ_x^+	$(=\lambda_x U_\tau‡/\nu)$	751	418	282; 292; 295
λ_x/h	—	1.98	1.67	1.72; 1.18; 0.95
λ_x/δ_ℓ	—	5.95	3.91	3.22; 2.78; 2.40

† Neither Wygnanski nor Itsweire & Van Atta measured the convection velocity of substructures. The present measured value of $\bar{U}_c^*$ ($= 0.66U_1$) at $y/h = 0.02$ has been used with their data.

‡ The friction velocity U_τ was not measured in any of these experiments; the magnitude of U_τ was estimated from the measurements of Mautner & Van Atta (1986). Their ensemble-averaged wall shear stress distribution indicates that the ratio U_τ/U_1 increases from 0.031 at the leading edge to 0.039 at the trailing edge. A nominal value of $U_\tau/U_1 = 0.033$ corresponding to the maximum spot height has been used.

TABLE 1. Streamwise spacing of substructures for MPS

of 172 for ϕ, in reasonable agreement with the value of 15.3° obtained from flow visualizations by Schubauer & Klebanoff (1956).

5.3. *Inclination of substructures*

To estimate the average inclination of the substructures in the (x, y)-plane, the convection-velocity distribution obtained at several values of y/h is used in conjunction with data obtained from the y-array. Since N_p deecreases with increasing y/h we focus only on those substructures that fall in the central region of the spot. In particular, substructures 3, 4, 5 are considered at $x_s = 52.5$ cm and 4, 5, 6, 7 at $x_s = 83$ and 113 cm. A reference wire is chosen ($y/h \approx 0.085$) in the y-array and the most probable time delay τ between the detection of a substructure at this location and that at any other location in the array is calculated. This time delay can be either positive or negative depending on whether the reference wire is below or above the other detection location. To obtain the average shape of a substructure, each time delay τ is converted to a lengthscale Δx using the transformation $\Delta x = -U_c\tau$. The distribution y/h *vs.* $\Delta x/h$ represents the average shape of the substructures in the (x, y)-plane as shown in figure 10(*a*). Note that the shape of substructures remains approximately the same for a considerable streamwise

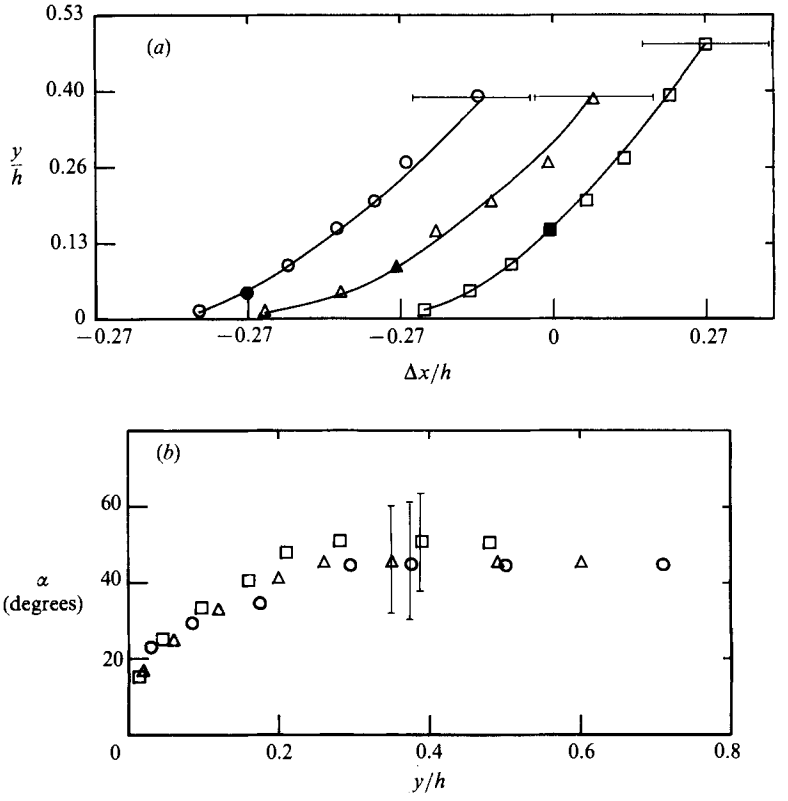

FIGURE 10. Average shape and inclination in the (x, y)-plane of substructures in the central region of the MPS. (*a*) Shape: ○, $x_s = 52.5$ cm; △, 83; □, 113. The filled symbol is the reference location. (*b*) Inclination: ○, $x_s = 52.5$ cm; △, 63; □, 113.

distance. Also, changing the reference wire location to $y/h \approx 0.38$ does not alter the shape of the curve. Using a cubic spline fit to the data for y *vs.* Δx, the average inclination α is calculated from

$$\alpha = \tan^{-1}\left[\frac{\partial(y)}{\partial(\Delta x)}\right].$$

Figure 10(*b*) shows the distribution of α as a function of y/h. The inclination is small ($\approx 18°$) near the wall and becomes constant ($\approx 45°$) for $y/h \geqslant 0.35$. The level of uncertainty shown in this figure is high ($\pm 25\%$ at $x_s = 52.5$ cm, $\pm 34\%$ at $x_s = 113$ cm) because of the relatively low sampling frequency used for the y-array data. Nevertheless, the trend of the data is unmistakable.

Comparison of these inclinations can be made with angles inferred from the (x, y)-plane photographs of an artificially induced turbulent spot deeveloping in a water tunnel (Gad-el-Hak *et al.* 1980, 1981; and Matsui 1980). The hairpin vortices which can be seen in the central regions of these photographs are inclined to about 18° near the wall and about 45° outside the boundary layer. Also, the (x, y)-plane photographs of the central region of a natural turbulent spot of Matsui (1980) indicate that the inclination of hairpin vortices is about 14° near the wall and 38° away from the wall. For the hairpin vortices artificially created by the injection of fluid in a water tunnel, Acarlar & Smith (1987*a*, *b*) report inclinations of 12° near the

wall and about 45° away from the wall. The numerical simulation study of the final stages of transition in a plane channel flow of Biringen (1984) indicates that the hairpin vortices are inclined to the main flow direction, the inclination increasing from 14° to 40° as the distance from the wall increases.

Head & Bandyopadhyay (1981) noted that vortex loops have a characteristic angle of about 40–50° in a turbulent boundary layer near the free stream and about 20° close to the wall. For a turbulent boundary layer, Fulachier *et al.* (1987) found that coolings have a constant inclination of about 47° when $y^+ \geqslant 80$. The previous observations and the present results suggest a close association between the spot substructures and hairpin vortices. It also reinforces the contention that the spot substructures are the basic modules of the turbulent boundary layer.

6. Streamwise variation of substructures

The previous sections have dealt with different characteristics of the substructures in the MPS and have indicated that the number of these substructures increases with x_s. It now seems appropriate to consider the way in which these substructures fit within the spot boundaries and provide a formula for relating the number of substructures to x_s. Since most of the detailed information has been obtained at the first streamwise station, our perceived view of a two-dimensional cut through the MPS is shown at this station. The overall boundary or envelope of the spot and the boundaries of the substructures are sketched in figure 11.

The spot envelope is essentially the locus of t_{LE} and t_{TE}, determined at various values of y. When the spot duration $(t_{TE}-t_{LE})$ is normalized by t_0 (the duration at $y \approx 0$) and plotted against y/h, the resulting distribution (not shown here) is similar to that reported by Wyngnanski *et al.* (1976). The height of the overhang near the leading edge is approximately equal to the laminar boundary-layer thickness, as noted by Gutmark & Blackwelder (1987).

As discussed in §3, the leading edge and trailing edge of individual substructures were identified at each wire location of the y-array by detecting heatings and coolings. A rough estimate of the height of each substructure has been inferred from the most probable time delay τ betwen the detection of the trailing edge of a substructure at a reference wire ($y/h = 0.085$) and that at any other location in the y-array (see §5.3). For each non-reference wire ($y/h = 0.18, 0.30, 0.38, 0.51, 0.71, 0.88$) the number of detections falling within the range 0.75τ–1.25τ relative to reference wire detections was determined. The height h_i of substructure i was identified with the value of y at which the number of detections for the non-reference wire first fell below 50% of the detections at the reference wire. Although the criterion is somewhat arbitrary, estimates of h_i (figure 11) fit convincingly within the spot envelope.

The most probable time interval and streamwise spacing between successive substructures are about 10.5 ± 0.7 ms and 31 ± 2 mm respectively. A convection velocity of $\bar{U}_c^* = 0.66U_1$ (at $y/h = 0.02$) was used to determine this spacing. The most probable spacing between the leading edge and trailing edge of a substructure was obtained by detecting heatings for substructures 2 and 3 and coolings for substructure 2. The probability of detecting heatings relative to the detected cooling was calculated. Two local peaks in the probability distribution identified the most probable locations of the leading edges (heatings) of substructures 2 and 3. The time interval between the two peaks, approximately equidistant from the reference location, was about 10 ms. The duration between the first peak and the reference

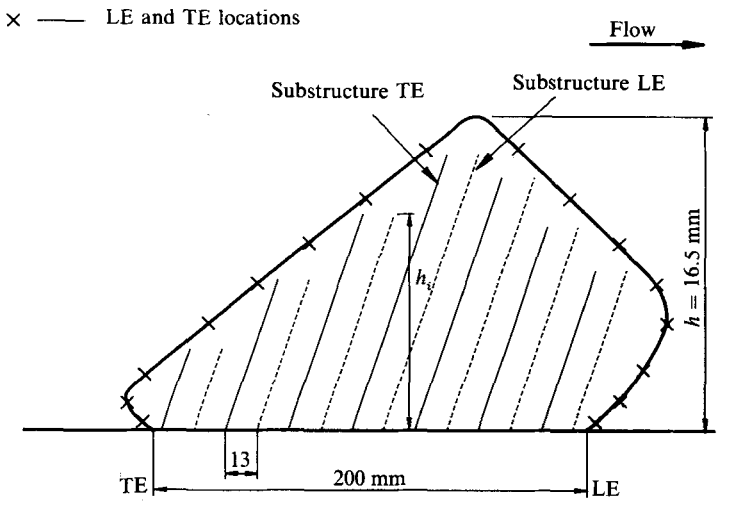

FIGURE 11. Cross-sectional cut through the MPS at $x_s = 52.5$ cm with the substructures arranged at their most probable location.

position yields the most probable duration t_w ($= 4.5 \pm 0.5$ ms) associated with substructure 2. The above procedure was then repeated for substructures 3 and 4 and substructures 4 and 5. These probability distributions indicated that t_w remained constant for all the combinations considered. Cursory checks made at the downstream stations showed that t_w does not depend on x_s. The most probable width $t_w \bar{U}_c^*$ of a substructure is 13 (± 1.5 mm). This spacing, together with an average substructure inclination of 45° were used in constructing figure 11.

The maximum number of substructures N_p^* in the MPS can be obtained from the ratio of the spot length L and the spacing λ_x between substructures. At a given x_s, the spot length L can be written as

$$L = (U_{LE} - U_{TE}) t_{TE} = \left(\frac{t_{TE}}{t_{LE}} - 1\right) x_s$$

since $x_s = U_{TE} t_{TE} = U_{LE} t_{LE}$. It follows that

$$N_p^* = \left(\frac{t_{TE}}{t_{LE}} - 1\right) \frac{x_s}{\lambda_x}. \tag{4}$$

A least-squares linear regression was carried out on the present data for N_p^* *vs.* $(t_{TE}/t_{LE} - 1)\, x_s$. Also included were the data for MPS + 1 and MPS − 1. This was done to improve statistical accuracy; MPS + 1 and MPS − 1 account for a significant number of spots (figure 2) and the convection velocity and spacing of substructures in these two spot populations are essentially the same as those for the MPS. The line in figure 12 is given by

$$N_p^* = \beta_1 \left(\frac{t_{TE}}{t_{LE}} - 1\right) x_s, \tag{5}$$

with $\beta_1 = 0.027$ mm^{-1} (± 0.001). The small standard deviation presumably reflects the constancy of λ_x. This value of β_1 implies that λ_x is 37 mm whereas the measured value of λ_x is 31 ± 2 mm. It should be noted however that N_p^* is the maximum number of substructures in the MPS, which typically occurs at about $y/h \approx 0.1$ (cf.

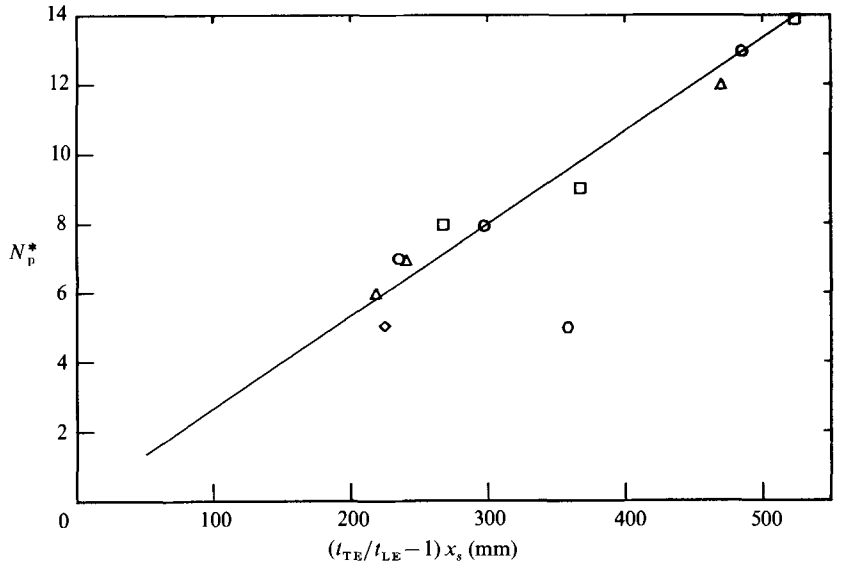

FIGURE 12. Streamwise growth of substructures. Present: ○, MPS; △, MPS−1; □, MPS+1; ⬡, Itsweire & Van Atta (1984); ◇, Wygnanski (1983).

figure 4). In estimating β_1 from (5), the values of t_{LE} and t_{TE} obtained at $y/h = 0.085$ were used. At this location, $\bar{U}_c^*$ is $0.78U_1$. This yields a value of $\lambda_x (= t_D \bar{U}_c^*)$ of 37 ± 2 mm, in excellent agreement with the value of λ_x inferred from β_1.

Since the ratio t_{TE}/t_{LE} is reasonably constant (our MPS data yielded a value of about 1.4 ± 0.04), relation (5) may be replaced by the simpler relation

$$N_p^* = \beta_2 x_s. \tag{6}$$

A least-squares fit to (6), using the present data, yielded $\beta_2 = 0.011$ (± 0.0013) mm^{-1}. Relations (5) and (6) should provide an approximate estimate for the number of substructures in other spot experiments, carried out with zero pressure gradient. In this context, Wygnanski's (1983) MPS point (figure 12) is in reasonable agreement with (5). The location of Itsweire & Van Atta's (1984) MPS point on figure 12 suggests that the number of substructures indicated by these authors may have been underestimated by a factor of 2; this discrepancy is reflected in the table.

7. Implications of previous results on a model of the spot

The delineation of figure 11 suggests that the flow within a spot could, in principle, be modelled by selecting an appropriate number of substructures or hairpin vortices. Apart from the number of vortices, other model parameters would include the streamwise distance between vortices, the average inclination of vortices to the wall, and the distance from the wall of the tips or heads of the vortices. The results of the previous sections provide all of this information as well as a knowledge of a suitable convection velocity for the vortices and the appropriate dependence of this velocity on the distance from the wall. However, no information has been obtained in the present study on the velocity field of the spot or, more pertinently from a modelling viewpoint, on the velocity and vorticity signatures of the substructures. Until this information is available, any attempt at modelling would be premature.

In the context of modelling, much encouragement can however be drawn from the numerical simulation of Leonard (1980) who used a three-dimensional vortex filament description of the vorticity field to compute the growth of a turbulent spot in a laminar boundary layer. The Biot–Savart law was applied to the vortex filaments and their images (an inviscid boundary condition was assumed at the wall). Good agreement was reported between the simulation and measured properties of the spot, such as velocities of the leading edge and trailing edge, away from the wall. Perry & Chong (1982) formulated a model for wall turbulence on the basis of a hierarchy of Λ-vortices with different heights, the particular Λ-vortex configuration having been inspired by visualizations (Perry *et al.* 1981) of trip-wire and turbulent-spot vortices. The Biot–Savart law was used to compute the velocity field, the resulting computations demonstrating that the vortices have the correct transport properties.

It is axiomatic that any proposed model must satisfy the time-averaged or ensemble-averaged properties of the flow to which it is applicable. For example, Perry & Chong's model yielded the logarithmic mean velocity profile as well as broadband turbulence intensities and spectra in a turbulent boundary layer. A turbulent-spot model, based on a suitable collection of substructures, should yield the measured ensemble-averaged properties of the spot. It is not difficult to show, at least qualitatively, that the assembly of substructures, as depicted in figure 11, is consistent with the ensemble-averaged temperature of the spot.

To this end, we have obtained the individual temperature signatures of each of the seven substructures that are delineated in figure 11. Conditionally averaged temperature distributions were obtained at $y/h = 0.17$ ($x_s = 52.5$ cm) for the MPS population (112) after aligning with respect to the detection instant (here corresponding to a sudden decrease in temperature). These distributions for each substructure (numbered) are shown in figure 13, each distribution having been calculated for one average substructure width (cf. §6, 13 ± 1.5 cm) on either side of the detection instant. The signatures have been located at positions separated by the distance shown in figure 11. It can be noted that the signatures join together in an almost smooth fashion (although a very slight kink can be detected at the junctions identified by the vertical lines in the figure). Also shown in figure 13 are the ensemble-averaged distributions obtained for the MPS population and the total spot population; for these averages, the alignment was with respect to the leading edge. It is clear that the MPS ensemble average represents a reasonable average through the individual signatures; equally plausible results (not shown here) were obtained at other values of y/h. One expects that there will be jitter in the arrival time, duration, inclination and height of individual substructures. This jitter will cause the erosion of the peaks and the filling in of the troughs in the individual signatures. Note that although the ensemble-averaged distribution for the MPS population is different from that of the total population, it fails to reflect the presence of the individual substructures, thus emphasizing the importance of the jitter. A realistic spot model would need to take account of this but there is little doubt that the MPS concept provides a more manageable environment than the total spot population for testing the model. It is of interest to observe that the peak temperature amplitude varies between individual signatures. The variation reflects in a rough manner the different heights of individual vortices (figure 11). The height variation suggests that vortices have been stretched at different rates. Conservation of heat considerations, similar to those used by Perry & Chong (1982), indicate that, at any given distance, the temperature increase associated with the vortex-induced flow is inversely pro-

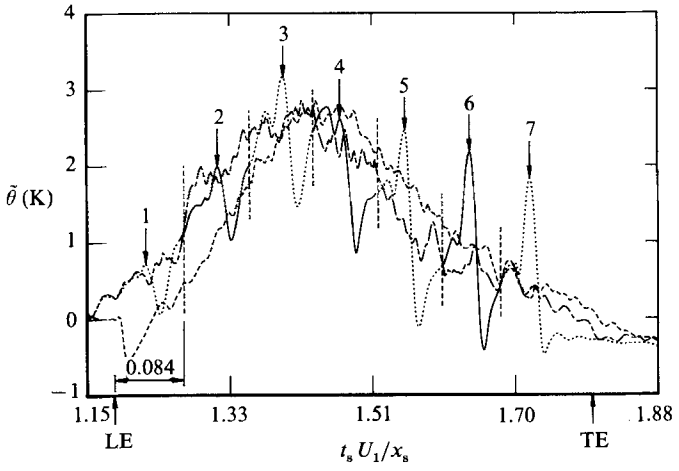

FIGURE 13. Comparison between conditional temperature distributions for the individual MPS substructures ($y/h = 0.17, x_s = 52.5$ cm) and the ensemble-averaged temperature distributions for the MPS population and the total spot population. Solid and broken curves are used for alternate substructures in the distributions of individual MPS substructures. Continuous curves: —·—, MPS population; – – –, total population.

portional to the vortex cross-sectional area. This implies that vortices that stretch further out into the spot would have a higher amplitude; this is in rough qualitative agreement with figure 13.

8. Concluding discussion

The results of the previous sections emphasize that the spatial growth of the turbulent spot is directly related to a streamwise increase in the number of substructures. The focus on the spot population with the most probable number of features has enabled the substructures to be identified and several of their characteristics to be determined. In particular, the convection velocity is the same for all substructures. In Matsui's (1980) sequence of hydrogen-bubble photographs in a natural spot, the time history of individual hairpin vortices can be observed. Using figure 5 of Matsui's paper, we estimate that each vortex travels at approximately the same convection velocity. The magnitude of this velocity is approximately equal to U_1, consistent with the fact that it is the tip or head of the vortex that is clearly identifiable in the photographs and that the head is always either at or above the edge of the local boundary-layer thickness.

The increase in the convection velocity with distance from the wall suggests that the substructures are stretched as they move away from the wall. This increase is consistent with the increase, measured by Acarlar & Smith (1987*b*), in the head of a hairpin vortex as it migrates away from the wall within a laminar boundary layer. The average inclination of the substructures is relatively shallow near the wall, increasing to about 45° away from the wall. There is qualitative similarity between the previous features and those pertaining to coolings in a turbulent boundary layer (Fulachier *et al.* 1987). This similarity strengthens the notion that the physical structures in the two flows are similar, but the interaction between structures is likely to be more significant in a turbulent boundary layer than in a spot. The possibility of interaction between substructures within a spot cannot be ruled out:

although the convection velocity of substructures that are found at a particular distance from the wall is the same, the tips of different substructures may be at different distances from the wall. It follows that the tips of adjacent substructures may travel at different velocities, hence increasing the possibility of amalgamation as discussed by Acarlar & Smith (1987*b*) in the context of hairpin vortices or the possibility, noted by Perry *et al.* (1981), that vortex loops at the rear of the spot may climb over those further downstream.

The suggestion that new substructures are formed near the trailing edge is not new. It was made by Matsui (1980) and Gad-el-Hak *et al.* (1981), on the basis of flow visualizations. Matsui suggested that the spot grows in the x-direction through the generation of new vortices at trailing edge and concluded that the difference in convection velocity between the leading and trailing edges was caused by this generation. Gad-el-Hak *et al.* attribute the growth of the spot in the (x, y)-plane to the appearance of new eddies, which 'typically occur only upstream of the existing ones, i.e. towards the trailing edge of the spot'. They also noted (in relation to their figure 5) that very little new turbulence appeared near the head of the spot, most of the activity occurring at its rear. Our observations of temperature traces from either the x-array or y-array of cold wires indicate that new signatures (i.e. a slow rise followed by a rapid cooling, see for example, figure 1 (*a*) tend to form primarily near the trailing edge and are often preceded by a laminar portion (i.e. fluid at the local temperature of the laminar boundary layer) of significant duration. New signatures are also observed near the leading edge but much less frequently than at the trailing edge. The previous observations suggest that the trailing edge, which is identified with the last turbulent-to-laminar interface, arrives at a particular x_s location with a relatively larger dispersion than the leading edge arrival time. Probability density functions were calculated for both the trailing- and leading-edge arrival times. At $x_s = 52.5$ cm, the ratio of the standard deviation of the leading-edge arrival time to the standard deviation of the trailing-edge arrival time is about 0.43 at $y/h = 0.085$ and at $y/h = 0.35$. A maximum value of 0.55 for this ratio is indicated by the data of Gutmark & Blackwelder (1987).

So far, no mention has been made of how the new vortices are created. The present measurements do not throw direct light on this. Previous flow visualizations (Elder 1960; Cantwell *et al.* 1978; Perry *et al.* 1981; Gad-el-Hak *et al.* 1981; Carlson, Widnall & Peeters 1982) clearly reveal the presence of low-speed streaks upstream of the rear edge of the spot. These streaks have approximately the same spanwise spacing (≈ 86 wall units according to Cantwell *et al.* 1978 and Perry *et al.* 1981) as found underneath a turbulent boundary layer and exhibit significant streamwise coherence. It has been proposed (e.g. Wallace 1982) that these streaks are formed by pairs of counter-rotating longitudinal vortices; the wall-attached legs of the hairpin vortices in a turbulent spot would provide such a streak formation mechanism. The existence of streaks seems to be a prerequisite for the bursting sequence described by Kim, Kline & Reynolds (1971) and presumably the creation of new vortices (e.g. Smith & Schwartz 1983; Smith & Metzler 1983; Acarlar & Smith 1987*b*). The convecting potential-flow field associated with the hairpin vortices could provide sufficient disturbances to initiate near-wall instabilities (and hence new vortices). Our observations that new (latest) substructures travel, almost as soon as they are created, with the same convection velocity as that of the earlier substructures, lends credence to the possibiity that there is a continuous generation mode, i.e. substructures that are just formed will themselves generate newer substructures and so on. It is of interest to recall that Sokolov, Antonia & Chambers (1986) found that

the potential-flow field associated with a spot initiated on one wall of a duct can trigger a second spot on the opposite wall, this latter spot propagating at the same convection velocity as the original spot.

From flow visualizations in a relatively low-Reynolds-number turbulent spot, Perry *et al.* (1980, 1981) provided an interesting hypothesis for the generation of new Λ or hairpin vortices as the spot develops. They conjectured that the spot propagates in the downstream direction in a domino-like manner while it grows laterally at the same time. The initial spot disturbance induces undulations in the spanwise vortex filaments. These undulations propagate laterally but the forward-leaning sections of the undulations, which have lifted away from the wall, generate disturbances in downstream vortex filaments through an induced backward flow. The streamwise increase in the number of Λ-vortices is consistent with the present increase in the number of substructures. However, Perry *et al.*'s conjecture that new vortices are generated at the leading edge differs from aforementioned evidence of Matsui (1980), Gad-el-Hak *et al.* (1981) and the present observations that new structures are mainly formed near the trailing edge. In Perry *et al.*'s scenario, vortices that are first formed are stretched to larger distances from the wall than those downstream, i.e. towards the leading edge. This implies a height distribution of vortices within the spot boundaries that seems at variance with the delineation of figure 11 near the upstream end of the spot. A possible scenario for the creation of structures with a height distribution consistent with that in figure 11 may be one that includes both the domino-like generation mechanism near the leading edge and the creation of new vortices near the trailing edge through instabilities of the low-speed streaks formed by downstream hairpin vortices. Although both generation mechanisms are self-perpetuating, the scenario ignores possible interactions between vortices and does not contain details of the interaction between vortices and the wall. In the latter context, the experiments of Acarlar & Smith (1987*b*) suggest a possible similarity between what happens in the near-wall region of a turbulent spot and the observations in a turbulent boundary layer. These authors compared the sudden ejection resulting from the interaction between a secondary vortex and the original hairpin vortex with the break-up stage of the bursting sequence. The relationship between a hairpin vortex and bursting, which is outside the scope of the present study, would be studied more profitably in the controlled environment of a turbulent spot than in a turbulent boundary layer.

It is finally worth remarking on the possible effect that a pressure gradient has on the spatial growth of a spot in the context of either enhancement or inhibition of new substructures. One would, for example, expect a favourable pressure gradient to inhibit new vortices (e.g. Kline *et al.* 1967 found that fewer 'ejections' occur when a favourable pressure gradient is applied to a turbulent boundary layer) and therefore reduce the difference between leading-edge and trailing-edge convection velocities or more precisely the average duration of the spot. This is indeed consistent with the influence of a favourable pressure gradient on a turbulent spot as observed by Wygnanski (1983) and Sankaran & Antonia (1988).

The support of the Australian Research Grants Scheme is gratefully acknowledged. R. A. A. and M. S. acknowledge the support of a Research Visitor grant by the Senate Research Committee, University of Newcastle. The help, with respect to computations, of Messrs D. K. Bisset and J. J. Smith was much appreciated.

REFERENCES

ACARLAR, M. S. & SMITH, C. B. 1987*a* A study of hairpin vortices in a laminar boundary layer. Part 1. Hairpin vortices generated by a hemisphere protruberance. *J. Fluid Mech.* **175**, 1–41.

ACALAR, M. S. & SMITH. C. R. 1987*b* A study of hairpin vortices in a laminar boundary layer. Part 2. Hairpin vortices generated by fluid injection. *J. Fluid Mech.* **175**, 43–83.

ANTONIA, R. A., CHAMBERS, A. J. & SANKARAN, R. 1985 A low speed wind tunnel to study the structure of a boundary layer with pressure gradient. *Rep. T.N. – FM* 85.1. Department of Mechanical Engineering, University of Newcastle.

ANTONIA, R. A., CHAMBERS, A. J., SOKOLOV, M. & VAN ATTA, C. W. 1981 Simultaneous temperature and velocity measurements in the plane of symmetry of a transitional turbulent spot. *J. Fluid Mech.* **108**, 317–343.

BANDYOPADHYAY, P. R. 1983 Turbulence spot-like features of a boundary layer. *Ann. N. Y. Acad. Sci.* **404**, 393–395.

BIRINGEN, S. 1984 Final stages of transition to turbulence in a plane channel flow. *J. Fluid Mech.* **148**, 413–442.

CANTWELL, B., COLES, D. & DIMOTAKIS, P. 1978 Structure and entrainment in the plane of symmetry of a turbulent spot. *J. Fluid Mech.* **87**, 641–672.

CARLSON, D. R., WIDNALL, S. E. & PEETERS, M. F. 1982 A flow-visualization study of transition in plane Poiseuille flow. *J. Fluid Mech.* **121**, 487–505.

CHEN, C.-H. P. & BLACKWELDER, R. F. 1978 Large-scale motion in a turbulent boundary layer: a study using temperature contamination. *J. Fluid Mech.* **89**, 1–31.

ELDER, J. W. 1960 An experimental investigation of turbulent spots and breakdown to turbulence. *J. Fluid Mech.* **9**, 235–246.

FALCO, R. E. 1977 Coherent motions in the outer region of turbulent boundary layers. *Phys. Fluids* **20**, S124–S132.

FLEISCHMANN, S. T. & WALLACE, J. M. 1984 Mean streamwise spacing of organized structures in transitional and developed bounded turbulent flows. *AIAA J.* **22**, 766–769.

FULACHIER, L., BENABID, T., ANSELMET, F., ANTONIA, R. A. & KRISHNAMOORTHY, L. V. 1987 Behaviour of coherent structures in a turbulent boundary layer with wall suction. In *Advances in Turbulence* (ed. G. Comte-Bellot & J. Mathieu), pp. 399–407. Springer.

GAD-EL-HAK, M., BLACKWELDER, R. F. & RILEY, J. J. 1980 A visual study of the growth and entrainment of turbulent spots. In *Laminar–Turbulent Transition* (ed. R. Eppler & H. Fasel), pp. 297–310. Springer.

GAD-EL-HAK, M., BLACKWELDER, R. F. & RILEY, J. J. 1981 On the growth of turbulent regions in laminar boundary layers. *J. Fluid Mech.* **110**, 73–95.

GAD-EL-HAK, M., BLACKWELDER, R. F. & RILEY, J. J. 1985 Visualization techniques for studying transitional and turbulent flows. In *Flow Visualization III* (ed. W. J. Yang), pp. 568–575. Hemisphere.

GUTMARK, E. & BLACKWELDER, R. F. 1987 On the structure of a turbulent spot in a heated laminar boundary layer. *Expts Fluids* **5**, 217–229.

HEAD, M. R. & BANDYOPADHYAY, P. 1981 New aspects of turbulent boundary-layer structure. *J. Fluid Mech.* **107**, 297–338.

ITSWEIRE, E. C. & VAN ATTA, C. W. 1984 An experimental investigation of coherent substructures associated with turbulent spots in a laminar boundary layer. *J. Fluid Mech.* **148**, 319–349.

JOHANSSON, A. V., HER, J.-Y. & HARITONIDIS, J. H. 1987 On the generation of high-amplitude wall-pressure peaks in turbulent boundary layers and spots. *J. Fluid Mech.* **175**, 119–142.

KIM, H. T., KLINE, S. J. & REYNOLDS, W. C. 1971 The production of turbulence near a smooth wall in a turbulent boundary layer. *J. Fluid Mech.* **50**, 133–160.

KLINE, S. J., REYNOLDS, W. C., SCHRAUB, F. A. & RUNSTADLER, P. W. 1967 The structure of turbulent boundary layers. *J. Fluid Mech.* **30**, 741–773.

LEONARD, A. 1980 Vortex simulation of three-dimensional spotlike disturbances in a laminar boundary layer. In *Turbulent Shear Flows II* (ed. L. J. S. Bradbury, F. Durst, B. E. Launder, F. W. Schmidt & J. H. Whitelaw), pp. 67–77. Springer.

MATSUI, T. 1980 Visualization of turbulent spots in the boundary layer along a flat plate in a water flow. In *Laminar–Turbulent Transition* (ed. R. Eppler & H. Fasel), pp. 288–296. Springer.

MAUTNER, T. S. & VAN ATTA, C. W. 1986 Wall shear stress measurements in the plane of symmetry of a turbulent spot. *Expts Fluids* **4**, 153–162.

MOTOHASHI, T. & BLACKWELDER, R. F. 1983 Decreasing the side wall contamination in wind tunnels. *Trans. ASME* I: *J. Fluids Engng* **105**, 435–438.

PERRY, A. E. & CHONG, M. S. 1982 On the mechanism of wall turbulence. *J. Fluid Mech.* **119**, 173–217.

PERRY, A. E., LIM, T. T., CHONG, M. S. & TEH, E. W. 1980 The fabric of turbulence. *AIAA Paper* 80-1358 (presented at AIAA 13th Fluid and Plasma Dynamics Conference, Snowmass, CO).

PERRY, A. E., LIM, T. T. & TEH, E. W. 1981 A visual study of turbulent spots. *J. Fluid Mech.* **104**, 387–405.

RILEY, J. J. & GAD-EL-HAK, M. 1985 The dynamics of turbulent spots. In *Frontiers in Fluid Mechanics* (ed. S. H. Davis & J. L. Lumley), pp. 123–155. Springer.

ROGERS, M. M. & MOIN, P. 1987 The structure of the vorticity field in homogeneous turbulent flows. *J. Fluid Mech.* **176**, 33–66.

SANKARAN, R. & ANTONIA, R. A. 1988 The influence of a favourable pressure gradient on the growth of a turbulent spot. *AIAA J.* (To appear.)

SANKARAN, R., CHAMBERS, A. J. & ANTONIA, R. A. 1986 The influence of a favourable pressure gradient on the growth of a turbulent spot. In *Proc. 9th Australian Fluid Mechanics Conf., Auckland*, pp. 342–345.

SCHUBAUER, G. B. & KLEBANOFF, P. S. 1956 Contributions on the mechanics of boundary-layer transition. *NACA Rep.* 1289.

SMITH, C. R. & METZLER, S. P. 1983 The characteristics of low-speed streaks in the near-wall region of a turbulent boundary layer. *J. Fluid Mech.* **129**, 27–54.

SMITH, C. R. & SCHWARTZ, S. P. 1983 Observation of streamwise rotation in the near-wall region of a turbulent boundary layer. *Phys. Fluids* **26**, 641–652.

SOKOLOV, M., ANTONIA, R. A. & CHAMBERS, A. J. 1980 A similarity transformation for a turbulent spot in a laminar boundary layer. *Phys. Fluids* **23**, 2561–2563.

SOKOLOV, M., ANTONIA, R. A. & CHAMBERS, A. J. 1986 A turbulent spot in a two-dimensional duct. *J. Fluid Mech.* **166**, 211–226.

SUBRAMANIAN, C. S., RAJAGOPALAN, S., ANTONIA, R. A. & CHAMBERS, A. J. 1982 Comparison of conditional sampling and averaging techniques in a turbulent boundary layer. *J. Fluid Mech.* **123**, 335–362.

TOWNSEND, A. A. 1956 *The Structure of Turbulent Shear Flow*, 1st edn. Cambridge University Press.

WALLACE, J. M. 1982 On the structure of bounded turbulent shear flow: a personal view. In *Developments in Theoretical and Applied Mechanics XI* (ed. T. J. Chung), pp. 509–521. Department of Mechanical Engineering, University of Alabama-Huntsville.

WYGNANSKI, I. 1983 On turbulent spots. In *Symp. on Turbulence: Proc. Seventh Symposium on Turbulence, September 1981* (ed. G. K. Patterson & J. L. Zakin), pp. 390–400. University of Missouri-Rolla.

WYGNANSKI, I., HARITONIDIS, J. H. & KAPLAN, R. E. 1979 On a Tollmien–Schlichting wave packet produced by a turbulent spot. *J. Fluid Mech.* **92**, 505–528.

WYGNANSKI, I., SOKOLOV, M. & FRIEDMAN, D. 1976 On a turbulent 'spot' in a laminar boundary layer. *J. Fluid Mech.* **78**, 785–819.

WYGNANSKI, I., ZILBERMAN, M. & HARITONIDIS, J. H. 1982 On the spreading of turbulent spot in the absence of a pressure gradient. *J. Fluid Mech.* **123**, 69–90.